



## Editor invited article

## Active compliant mechanisms for optimized actuation by LCE-based artificial muscles



Wenhui Chen, Ruicheng Wang, Ke Liu\*

Department of Advanced Manufacturing and Robotics, Peking University, Beijing, 100871, China

## ARTICLE INFO

## Keywords:

Active compliant mechanisms  
Smart materials  
Liquid crystal elastomer  
Soft actuator

## ABSTRACT

Compliant mechanisms leverage deformation of materials for precise, lightweight solution to transfer force and motion. By incorporating smart materials, active compliant mechanisms are formed with self-embedded actuation source. Here, we propose lightweight active compliant mechanisms that mimic biological joints, which are capable of transmitting displacements and forces from the linear contraction of artificial muscles into desired magnitudes and directions using a compact structural design. The artificial muscles are braided from liquid crystal elastomer (LCE) fibers and heating threads, competent of generating large force and stroke. Meanwhile, the compliant mechanisms are designed by topology optimization to imitate the functions of biological joints. Combining the braided artificial muscles and optimized compliant mechanisms, these active compliant mechanisms effectively achieve transmission of centralized linear actuation into multiple and various output motions, which is verified by both numerical simulations and experiments. Furthermore, we demonstrate that the active compliant mechanisms can be used for potential surgical procedures such as in-body grasping, cavity dilation, drug delivery, and suturing. The demonstrated biomimetic motions of the active compliant mechanisms hold significant potential for applications in medical devices and soft robots.

## 1. Introduction

Compliant mechanisms refer to mechanisms that output motions through the deflection of part or all of their flexible components (Zhu et al., 2020; Howell, 2012; Zhang and Zhu, 2018). Within elastic deformation range, compliant mechanisms are usually manufactured in one piece, resulting in advantages such as high precision, light weight, and low cost (Liu et al., 2019a,b; Araromi et al., 2020; Odhner et al., 2014; Langelaar, 2016). Applications of compliant mechanisms have expanded into fields such as automotive (Mackertich-Sengerdy et al., 2023; Karakus and Tanik, 2018), aerospace (Fowler et al., 2011; Zirbel et al., 2017), healthcare (Thomas et al., 2021; Kota et al., 2005), etc.

To achieve desired functionality, compliant mechanisms need delicate structural designs. Topology optimization is a commonly employed computational tool for the delicate design of compliant mechanisms by optimizing output while constraining material usage (Bendsøe and Sigmund, 2004; Bharti and Frecker, 2008; Zhu et al., 2018; Li et al., 2022). Most algorithms commonly employed to solve topology optimization problems rely on finite element (FE) analysis routines that utilize linear triangles and bilinear quadrilateral meshes (Zhang et al., 2018; Jia et al., 2023; Liu and Paulino, 2019; Wallin and Tortorelli, 2020; Chen et al., 2018). The linear triangles and bilinear quadrilateral

meshes often lead to weak connections and non-smooth boundaries in the optimized structure (Andreassen et al., 2011; Sigmund, 2001; Wallin and Tortorelli, 2020). To get robust connections and smooth boundaries in optimized compliant mechanisms, polygonal meshes are adopted in topology optimization, which are more suitable for manufacturing and application than traditional meshes (Pereira et al., 2011; Chandrasekhar et al., 2019; Chen et al., 2022; Zhang and Zhou, 2018). Therefore, we utilize polygonal meshes in the topology optimization of active compliant mechanisms in this work.

Although topology optimized compliant mechanisms are lightweight and effective, the weight and efficiency of the mechanism from a holistic view also depends on the actuation sources. Smart materials are exactly such kind of light-weight actuation source that respond to physical (Kim and Matsunaga, 2017; Ke et al., 2018; Soto et al., 2022; Lu et al., 2016; Weng et al., 2016; Bisoyi and Li, 2022; Chen et al., 2023) or chemical stimuli (Yu et al., 2017; Tang et al., 2021; Fu et al., 2022; Ying et al., 2021; Yu et al., 2016). Among various smart materials, the liquid crystal elastomers (LCEs) have attracted increasing attention due to the reversible muscle-like contraction (Kotikian et al., 2021; Wu et al., 2023; Liu et al., 2021; Wu et al., 2021; Li and Zhang, 2023; Kim et al., 2017; Wang et al., 2017; Javadzadeh et al., 2023).

Invited Editor: Yihui Zhang.

\* Corresponding author.

E-mail address: liuke@pku.edu.cn (K. Liu).

<https://doi.org/10.1016/j.mechmat.2023.104879>

Received 21 October 2023; Received in revised form 27 November 2023; Accepted 29 November 2023

Available online 15 December 2023

0167-6636/© 2023 Elsevier Ltd. All rights reserved.

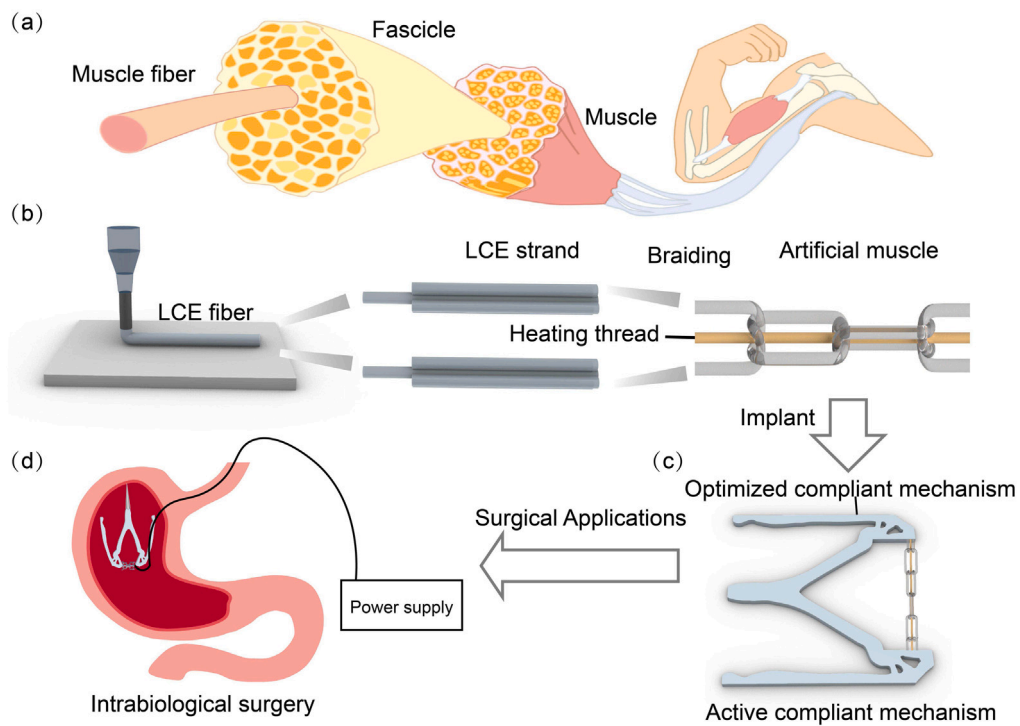


**Fig. 1. Manufacturing and potential application of active compliant mechanisms.** (a) Schematic of hierarchical structure of natural muscles. (b) Manufacturing process of braided artificial muscle bundle. (c) Schematic of active compliant mechanism. (d) Potential application of active compliant mechanisms in intrabiological surgery.

To improve the actuation performance, the diameter of LCE actuators were reduced to fibers for increased power density and actuation frequency (He et al., 2021; Wang et al., 2023; Javadzadeh et al., 2023; Roach et al., 2019). However, LCE fibers cannot generate enough force for most practical applications. It remains an open question how to incorporate LCE fibers with proper heating element(s) to create effective artificial muscles with large stroke and force.

In this paper, we develop economical, effective, and lightweight active compliant mechanisms, by combining LCE based artificial muscles with topologically optimized compliant mechanisms. To make the linear artificial muscles, we braid LCE strands consisting of LCE fibers with heating thread into architected bundles, inspired by the hierarchical structure of natural muscles (Kim et al., 2022; Madden et al., 2004) (Fig. 1a,b). To achieve optimized output actuation from the compliant mechanisms, we utilize a topology optimization approach employing polygonal meshes to design compliant mechanisms that transmit self-embedded linear actuation in various directions (Fig. 1c). By integrating the braided artificial muscles into the optimized compliant mechanisms as self-embedded actuation sources, these active compliant mechanisms output desired actuation upon contraction of the LCE. We verify the effectiveness of the proposed active compliant mechanisms by both numerical simulations and experiments, for a number of cases including converting horizontal linear contraction into gripping force, and transforming vertical contraction into forward or backward horizontal motion. The experimental samples of active compliant mechanisms are 3D printed using the thermoplastic polyurethanes (TPU) material. Finally, we demonstrate the potential application of these active compliant mechanisms for remote surgical operations by in vitro experiments involving grasping, cavity dilation, drug delivery, and suturing.

## 2. Manufacturing of braided artificial muscle bundles

### 2.1. Preparation of the LCE ink

The LCE ink is made by mixing (1,4-Bis-[4-(3-acryloyloxypropoxy)benzoyloxy]-2-methylbenzene) (RM257) (Wilshire Technologies, 95%),

EDDET (Sigma-Aldrich, 95%), dipropylamine (Sigma-Aldrich, 98%), (2-hydroxyethoxy)-2-methylpropiophenone (Irgacure 2959, Sigma-Aldrich, 98%), RhB (Sigma-Aldrich), and methylene chloride (Sinopharm, CH<sub>2</sub>Cl<sub>2</sub>). RM257 (HWRK Chem, 8.2404 g, 14 mmol) is dissolved in 50 ml of dichloromethane. Then, chain extender EDDET (2.1876 g, 12 mmol) and catalyst dipropylamine (0.100 g, 1 mmol–5 mmol) are added into the mixture dropwise. The solution is stirred at room temperature overnight. After that, photoinitiator (Irgacure 651, Medkoo, 0.0500 g, 0.2 mmol) is added into the solution. Then, the mixture is left in an oven of 85 °C for 24 h to allow complete evaporation of the solvent, and then we get the LCE ink for 3D printing.

### 2.2. Fabrication of the braided artificial muscle bundles

The LCE ink is put into a syringe loaded on a custom direct ink writing 3D printer. The LCE fibers are printed with a speed of 2 mm/s at temperature of 45 °C. The flow rate is controlled by regulating the air pressure applied on the syringe. After printing, fibers are removed from build plate and placed under a UV lamp of 365 nm wavelength for 1 h curing. Artificial muscle bundles are manually braided with 16 strands of LCE fibers and several (1–7) heating threads.

### 2.3. Improvement on actuation force of braided artificial muscle bundles

The 3D printed LCE fibers exhibit actuation strain around 32% when heated from 30 °C to 120 °C at a rate of 24 °C/min (Fig. 2a). Although the 3D printed LCE fibers exhibit a medium actuation strain, they present a tensile strength of about 0.8 MPa, obtained from the uni-axial mechanical tests conducted on a Universal Mechanical Testing System (Series F, Mark-10) with a 50N loading cell (Fig. 2b).

Each braided artificial muscle bundle consists of 16 LCE fibers and 1 stainless steel fiber yarn. Applying continuous current from 0.2 A to 0.8 A by a precision variable adjustable power supply (2200-50-3, ITECH), the actuation force of one braided artificial muscle bundle increases to about 0.3N in a quadratic trend with two sides fixed. This trend shows that the actuation force of braided artificial muscle bundles

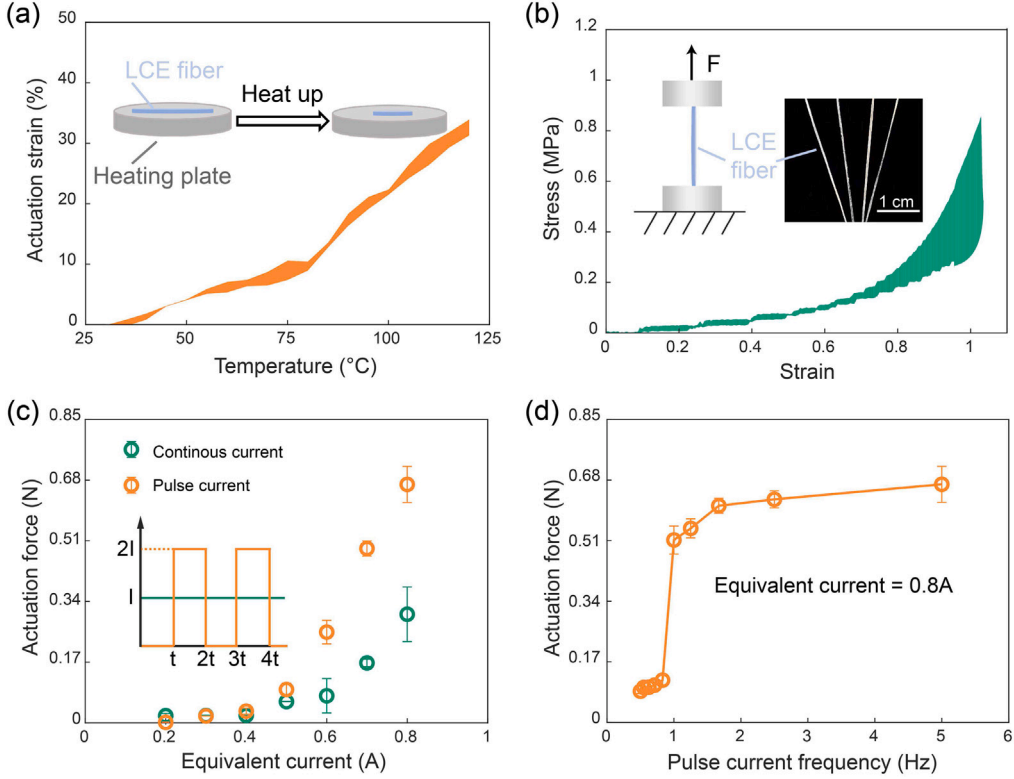


**Fig. 2. Actuation performance of individual LCE fiber and the braided artificial muscle bundle.** (a) The actuation strain of the LCE fiber under different temperature. The shading area in (a) and (b) refers to one standard deviation. (b) The stress-strain curve of the LCE fiber. (c) Actuation force of the braided artificial muscle bundle under continuous current and pulse current. The inset shows the details of the continuous current and the pulse current. The error bars extend to one standard deviation. (d) Actuation force of the braided artificial muscle bundles under pulse current of 0.8 A with different frequency. The error bars extend to one standard deviation.

is proportional to the input power. To further enlarge the actuation force, we introduce the pulse heating strategy that achieves the peak magnitude of current by 100%. To avoid overheating, we only keep this power-on stage for a short period, followed by a period of same duration without electric charge (i.e., the power-off stage). As a result, under the same average input power, the pulse heating strategy boosts the actuation force by a 100% increase compared to that of continuous current, reaching 0.66 N (Fig. 2c). Meanwhile, as the pulse current frequency increases, the actuation force of the braided artificial muscle bundle also increases, attributed to the shorter power-off interval that facilitates enhanced heat accumulation (Fig. 2d). Nevertheless, we do not rise the equivalent current beyond 0.8 A to prevent overheating and local fusion of the LCE strands.

To avoid large current in each heating thread, we increase the number of heating threads in the braided artificial muscle bundle. Adding the number of heating threads enables a higher amount of heat generation, thereby improving the actuation force, also effectively reducing the possibility of localized overheating. We introduce new heating threads in two different ways: (1) inserting heating threads in parallel with the original heating thread (inside); (2) adding heating threads in parallel with the LCE strand (outside), as illustrated in Fig. 3b-c. By these two ways, we make braided artificial muscle bundles with 2,3,4 heating threads with extra inside heating threads (1,2,3) (Fig. 3b) and braided artificial muscle bundles with 3,5,7 heating threads with extra outside heating threads (2,4,6) (Fig. 3c).

When subjected to the same total input current of 0.8 A, the incorporation of inserted heating threads in the artificial muscle bundle results in a notable reduction in the actuation force compared to the original bundles (Fig. 3d). The decrease in actuation force is attributed to a reduction in input heat caused by the shunt of the current by contact between heating threads. Nevertheless, inserting extra heating threads in braided artificial muscle bundles increases the maximum

tolerable current. When heated by the current of 0.5A/per heating thread, braided artificial muscle bundles with 3 extra inside heating threads and 2 extra outside heating threads demonstrate higher actuation force than that of one heating thread due to the amplified input heat (Fig. 3e). To maximize the actuation force of the braided artificial muscle bundles, we compare their actuation forces under the stimulation of various input currents. Under a total input current of 1.6 A, the braided artificial muscle bundle with 2 extra outside heating threads exhibits actuation force over 1N, beyond the majority of the artificial muscles with the same size (Fig. 3f). Therefore, we choose artificial muscles with 2 extra outside heating threads as the actuation source for our active compliant mechanisms.

### 3. Design of compliant mechanisms

On the basis of braided artificial muscle bundles being the actuation source, we proceed to design two sets of compliant mechanisms to form active compliant mechanisms working like biological joints. One set outputs the opposite displacement at a sharp angle to the input direction (A,B in Fig. 4), and the other set outputs displacement orthogonal to input direction (C,D in Fig. 4). Based on the design goal, we sketch all the boundary conditions on the right of Fig. 4, where the “x” markers refer to pin supports that fix all degrees of freedom, and the “o” markers refer to roller supports with only one degree of freedom.

We employ topology optimization to obtain the desired compliant mechanisms. Assuming our input braided artificial muscle bundle is a linear strain based actuator, which can be modeled as a spring with stiffness  $k_{in}$  and a force  $F_{in}$ . The goal of the optimization problem is to maximize the displacement  $U_{out}$  performed on a workpiece idealized by a spring with stiffness  $k_{out}$ . Different initial designs result in output forces and displacements with different directions and amount. For instance, the design parameters  $k_{in}$  and  $k_{out}$  have impacts on the input

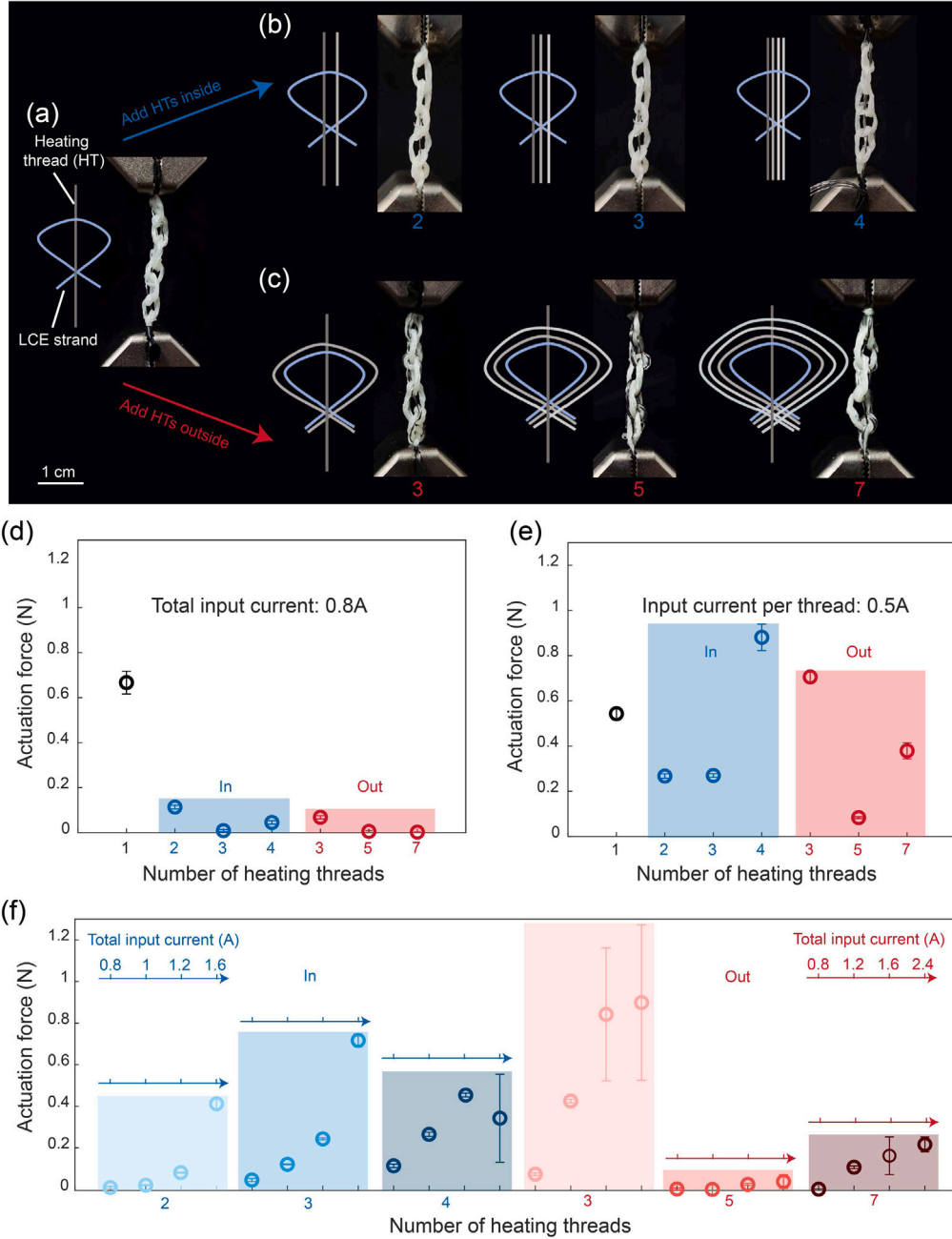


**Fig. 3. Actuation performance of braided artificial muscle bundle with refined braiding.** (a) Schematic of the original braiding style and its photograph. (b)-(c) The braiding styles: (b) adding inside heating threads and (c) adding outside heating threads. (d) The actuation force of the braided artificial muscle bundle under total input pulse current of 0.8 A. (e) The actuation force of the braided artificial muscle bundle under total input pulse current of 0.5 A per heating thread. (f) The actuation force of braided artificial muscle bundles under different total input pulse current. The error bars in (d)-(f) refer to one standard deviation.

displacement and  $U_{out}$  respectively. By specifying different values of  $k_{out}$  we can control the displacement amplification. Under small deformation assumption with linear elastic analysis, if we specify a low value of  $k_{out}$  we get large output displacements and vice versa. In order to maximize the output work on the spring, the available material must be distributed in structurally most efficient way. An optimization problem incorporating these ideas is formulated as:

$$\begin{aligned} & \text{Max}_{\rho} U_{out}, \\ & \text{s.t. : } \mathbf{r} = \mathbf{0}, \\ & \sum_{e=1}^N v_e \rho_e \leq V, 0 < \rho_{min} \leq \rho_e \leq 1, e = 1, \dots, N. \end{aligned}$$

where  $\mathbf{r}$  is the finite element residual for the analysis problem with the applied load  $F_{in}$ . We then solve this problem in 4 sets of design scenarios by the Matlab software “PolyTop” using polygonal meshes (Talischi et al., 2012a,b). The results are shown in the left of Fig. 5. We further apply post-processing on the edges of the optimized compliant mechanisms and extrude the 2D designs into 3D models for the following FE simulation and 3D printing. The post-processing method uses spline curves to fit the edges of the optimization results as shown in the right of Fig. 5. Based on the experimental and numerical results, we did not observe noticeable impact on the performance of the compliant mechanism by this post-processing procedure.

To verify if the optimized compliant mechanisms achieve our design goals, we import the 3D models into the commercial software

	Object inverters	Boundary conditions
A		
B		
C		
D		

**Fig. 4. Design of compliant mechanisms.** The design goal and boundary conditions of compliant mechanisms. Designs A and B output the opposite displacements at a sharp angle to the input direction. Designs C and D output the opposite displacement orthogonal to input direction.

ABAQUS/Static (Dassault Systèmes) to perform the function of transforming actuation. In the simulation, we adopt the material properties of the 3D printed TPU obtained from the uni-axial tensile experiments of six dog-bone samples (SI, Figure s1). We employ the tetrahedral mesh and typical quadratic accuracy tetrahedral continuum elements with 10 nodes (C3D10) for the nonlinear analysis.

The results of the nonlinear FE simulation verify that the optimized compliant mechanisms effectively achieve the desired displacement output. The optimized designs present nearly linear relationship between  $U_{in}$  and  $U_{out}$ . When the compliant mechanism A is subjected to an input force of 1 N, it converts a 5 mm internal contraction in the x-direction to a displacement of 7 mm in the negative y-direction plus a displacement of 2 mm in the positive x-direction (Fig. 6a-c). For the compliant mechanism B, it outputs a larger displacement of 10 mm in the negative x-direction plus a smaller displacement of 5 mm in the positive y-direction with a input displacement of 6.5 mm (Fig. 6d-f). As for the other set of compliant mechanisms with orthogonal input and output, the compliant mechanism C exhibits a negative x-direction displacement of 22 mm when subjected to an input force of 0.2 N along the y-direction. We observe that the input displacement for compliant mechanism C is greater than its resulting output displacement (Fig. 7a-c). Similarly, to achieve the same output displacement in the positive x-direction, the compliant mechanism D needs larger input displacement in y-direction than compliant mechanism C (Fig. 7d-e). Meanwhile, the required input displacement for compliant mechanism D is about twice of the output displacement (Fig. 7f).

To validate the results of simulation, we manufacture these compliant mechanisms by 3D printing and conduct experimental tests to assess their performance. The experimental results show that the performance

of 3D printed compliant mechanisms is in line with our expectations and consistent with the simulation results. As shown in Fig. 8a, when we push the left point of compliant mechanism A along the x-axis direction, the two rightmost points move in a direction inclined 45° to the input direction (Fig. 8a, Movie S1), which is consistent with the simulation results. And the displacement in negative y-axis direction is also larger than that in the positive x-axis direction which is also consistent with the simulation result. When we push the left point of compliant mechanism B in the same direction, the two rightmost points move along the opposite route with compliant mechanism A (Fig. 8b, Movie S2).

In the case of compliant mechanism C, when we immobilize the left two points and shorten the distance between the two right points, the center point on the left side moves in the direction of the negative x-axis (Fig. 9a-c, Movie S3). Similarly, for compliant mechanism D, the center point on the left side moves in the direction of the positive x-axis when the distance between the two right points is shortened (Fig. 9b, Movie S4). In general, not only do the direction of experimental output displacements align with the simulation results, but also the deformation states of compliant mechanisms in experiments are consistent with the simulation results which meet our design goals.

## 4. Results and discussion

### 4.1. Performance of active compliant mechanisms

The active compliant mechanisms generate linear actuation in various directions by transmitting the contraction of braided artificial muscle bundle induced by the current. This actuation mechanism enables

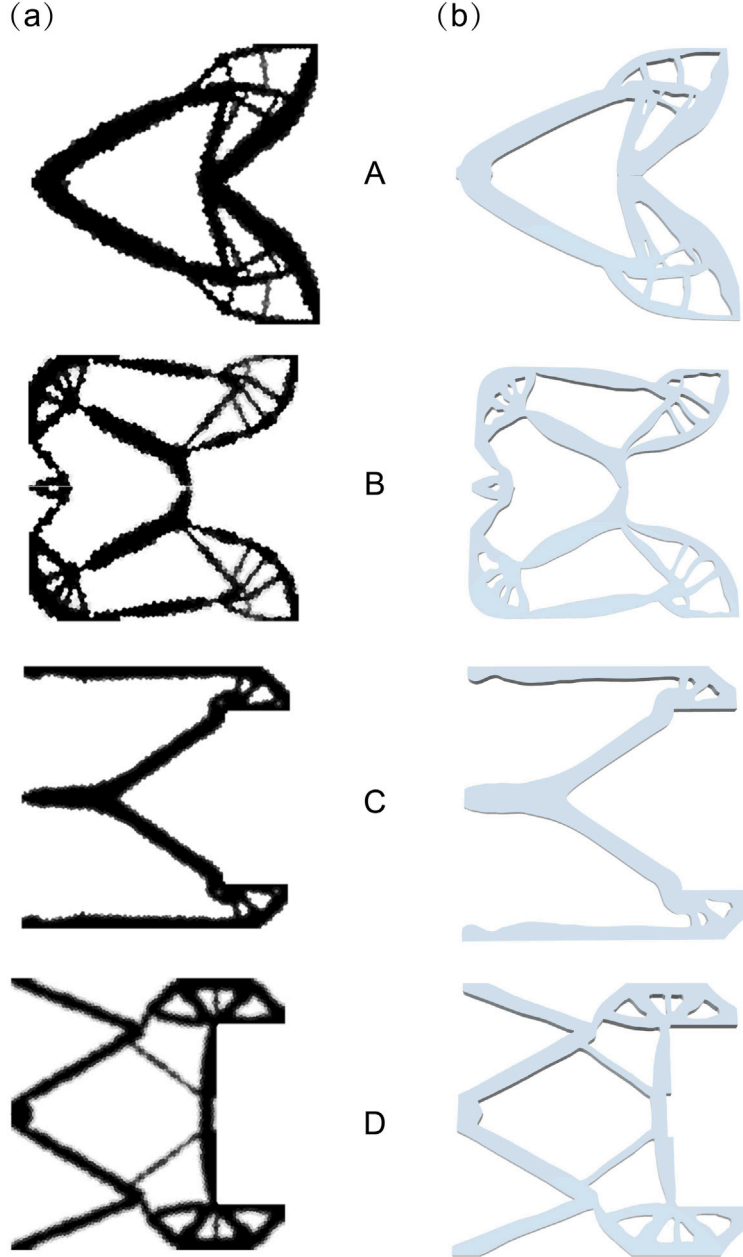


**Fig. 5. Optimized compliant mechanisms.** (a) The images of the optimized compliant mechanisms by polygonal mesh based topology optimization. (b) The rebuilt 3D models of the optimized compliant mechanisms.

remote controlling of the active compliant mechanisms. Meanwhile, the reversible actuation of LCE imparts the active compliant mechanisms with the capability to perform reversible deformation. When the thickness of the compliant mechanism is smaller than 2 mm, out-of-plane deformation could occur. However, the out-of-plane deformation can be mitigated by increasing the thickness of the compliant mechanisms. In our experiments, by printing the compliant mechanisms with a 3 mm thickness, the out-of-plane deformation becomes negligible.

Upon activating a pulse current of 3.2 A, the braided artificial muscle bundle contracts, dragging the left point of compliant mechanism A. Consequently, the two rightmost points exhibit similar motion patterns to those observed in previous experiments and retract to the original position after cutting off the current (Fig. 10a, Movie S5). With same current input, compliant mechanism B outputs the linear actuation in the opposite direction (Fig. 10b, Movie S6) and the other set of

active compliant mechanisms (compliant mechanism C,D) perform a pair of linear actuation in opposite direction along x axis (Fig. 10c,d, Movie S7,8). These phenomena indicate that, our active compliant mechanisms transmit desirable linear actuation in various direction with only current stimulation.

We demonstrate potential application of the active compliant mechanisms for *in vitro* surgical scenarios. When activated by electric current remotely, the active compliant mechanism A seizes and manipulates an irregular object, functioning as a live gripper that is adapted to the internal environment of organisms (Fig. 11a, Movie S9). With the opposite output, the active compliant mechanism B dilates a possible cavity channel when stimulated (Fig. 11b, Movie S10). For another set of active compliant mechanisms, through remote electrical stimulation (Fig. 11c, Movie S11), active compliant mechanism C achieves precise wound administration (Fig. 11d, Movie S12), while active compliant

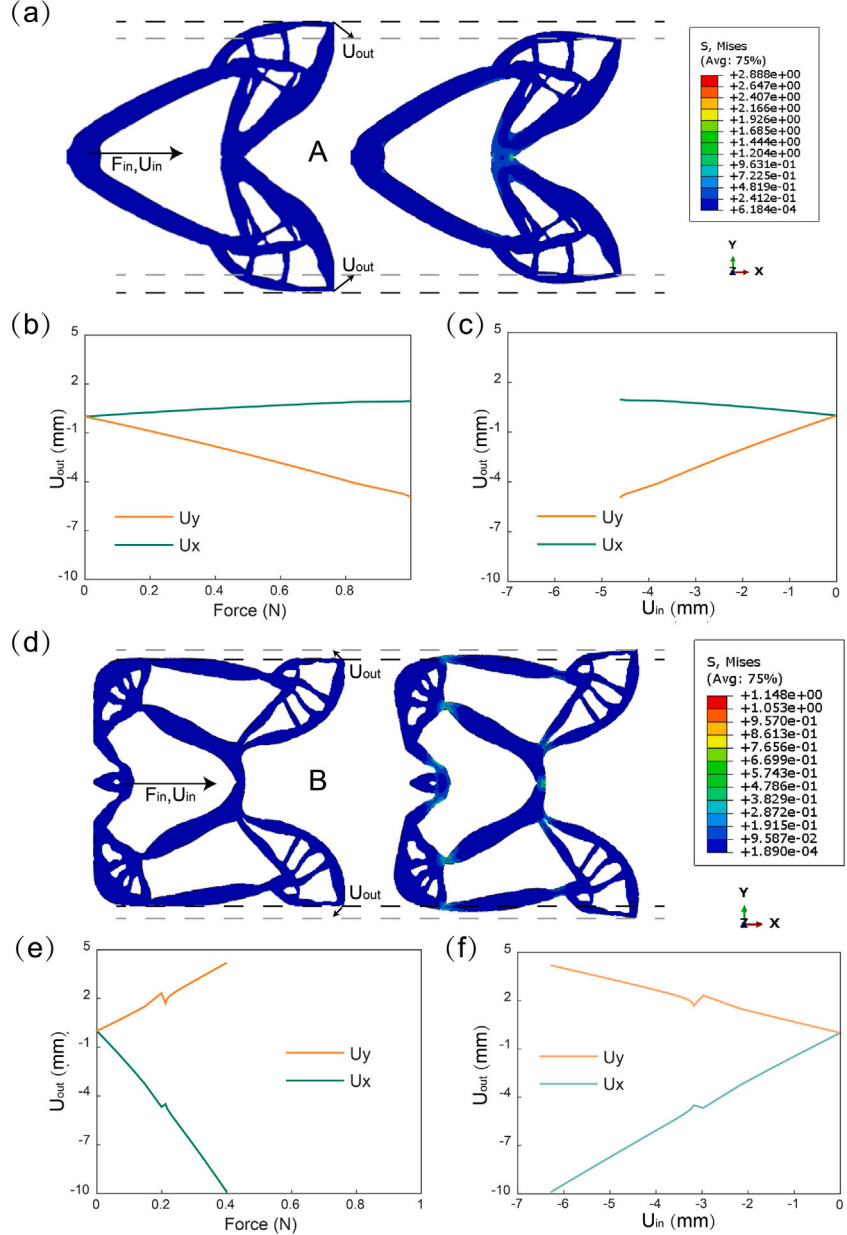


**Fig. 6. Simulation results of active compliant mechanisms A and B.** (a) The stress distribution of the compliant mechanism A before and after actuation under nonlinear large deformation analysis. The relation between output displacement of compliant mechanism A with (b) the input force (c) and input displacement. (d) The stress distribution of compliant mechanism B before and after actuation. The relation between output displacement of compliant mechanism B with (e) the input force (f) and input displacement.

mechanism D performs traction of suture. With these active compliant mechanisms, surgery within the organism can be completed through remote controlling, which could significantly reducing surgical costs and failure rates.

## 5. Conclusions

In this study, we integrate the braided artificial muscle bundles with optimized compliant mechanisms to create bio-inspired active compliant mechanisms, which is capable of transmitting linear actuation into various outputs. By braiding the LCE fibers and heating threads into architected artificial muscle bundles, we obtain lightweight

and soft actuators capable of generating large forces and stroke. Employing polygonal mesh based topology optimization, we design optimized compliant mechanisms. Combining these components, the active compliant mechanisms work as biological joints, showing the ability to achieve reversible actuations in multiple directions triggered by electric current. Compared to traditional actuation mechanisms, the bio-inspired active compliant mechanisms have a significantly simplified structure to output multi-directional actuations, demonstrating great application prospects in medical devices and soft robots. Looking ahead, we plan to incorporate large deformation analysis ([Li et al., 2022](#)) and 3D design domain ([Ansola et al. \(2010\)](#), [Liu and Tovar \(2014\)](#)) in our optimization of active compliant mechanisms, so that their accuracy and complexity can be further improved.

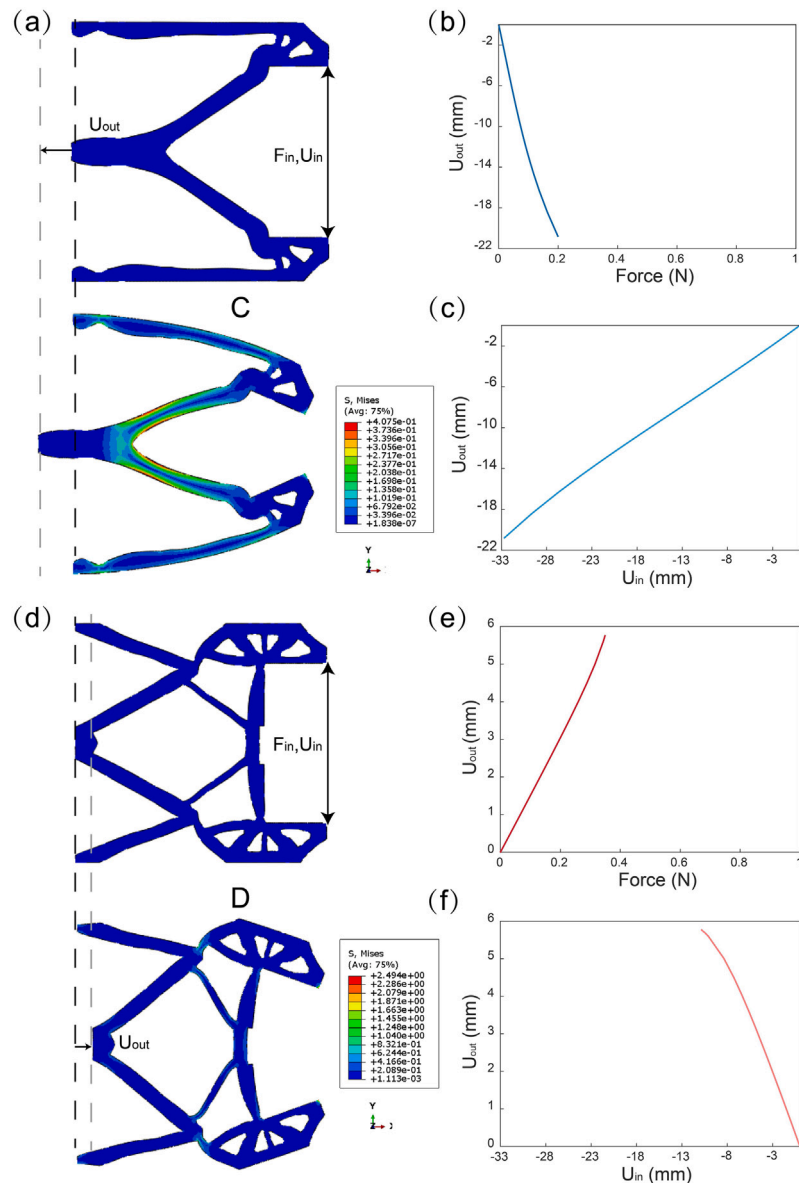


**Fig. 7. Simulation results of compliant mechanisms C and D.** (a) The stress distribution of compliant mechanism C before and after actuation. (b) The relation of output displacement and input force. (c) The relation of output displacement and input displacement. (e) The stress distribution of compliant mechanism D before and after actuation. (f) The relation of output displacement and input force. (g) The relation of output displacement and input displacement.

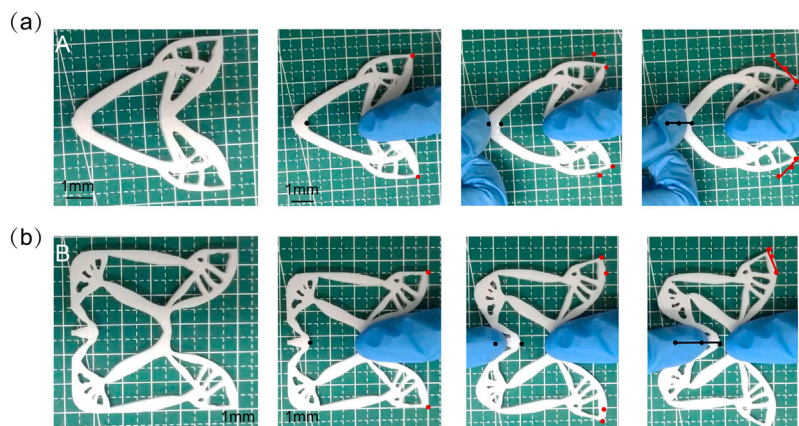


**Fig. 8. The deformation process of compliant mechanism A and compliant mechanism B.** (a) The deformation process of compliant mechanism A. (b) The deformation process of compliant mechanism B.

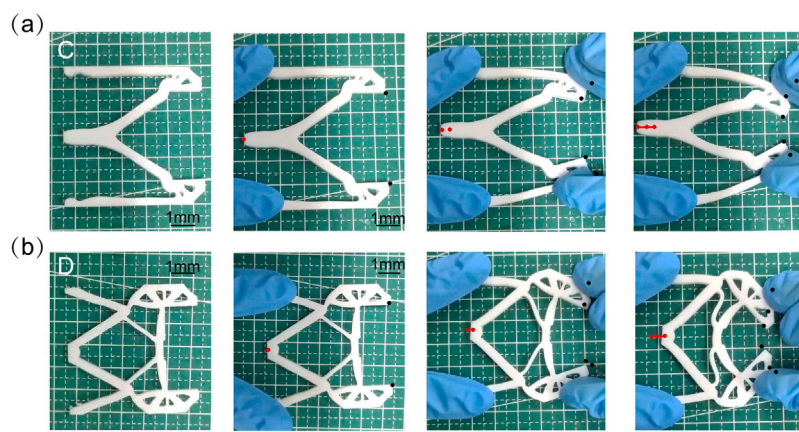


**Fig. 9. The deformation process of compliant mechanism C and compliant mechanism D. (a)** The deformation process of compliant mechanism C. **(b)** The deformation process of compliant mechanism D.

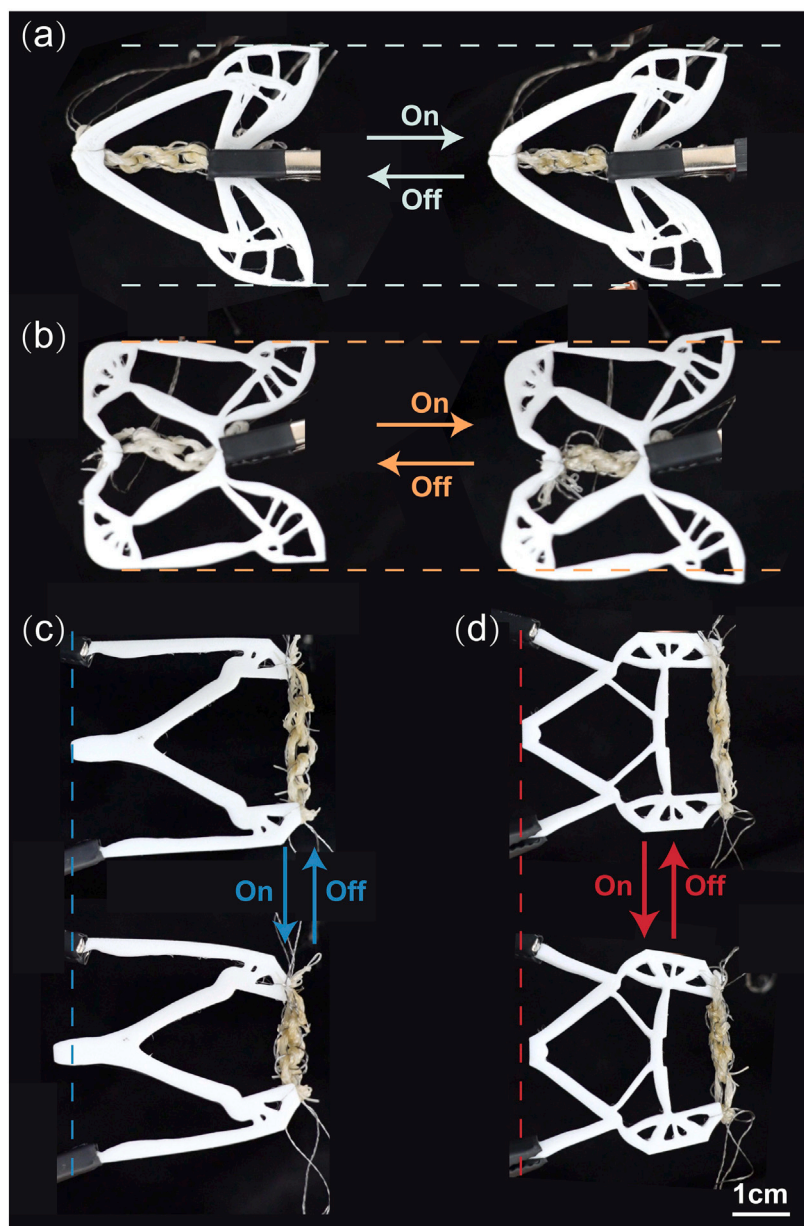


**Fig. 10. The deformation process of the active compliant mechanisms. (a)** The deformation process of active compliant mechanism A. **(b)** The deformation process of active compliant mechanism B. **(c)** The deformation process of active compliant mechanism C. **(d)** The deformation process of active compliant mechanism D.

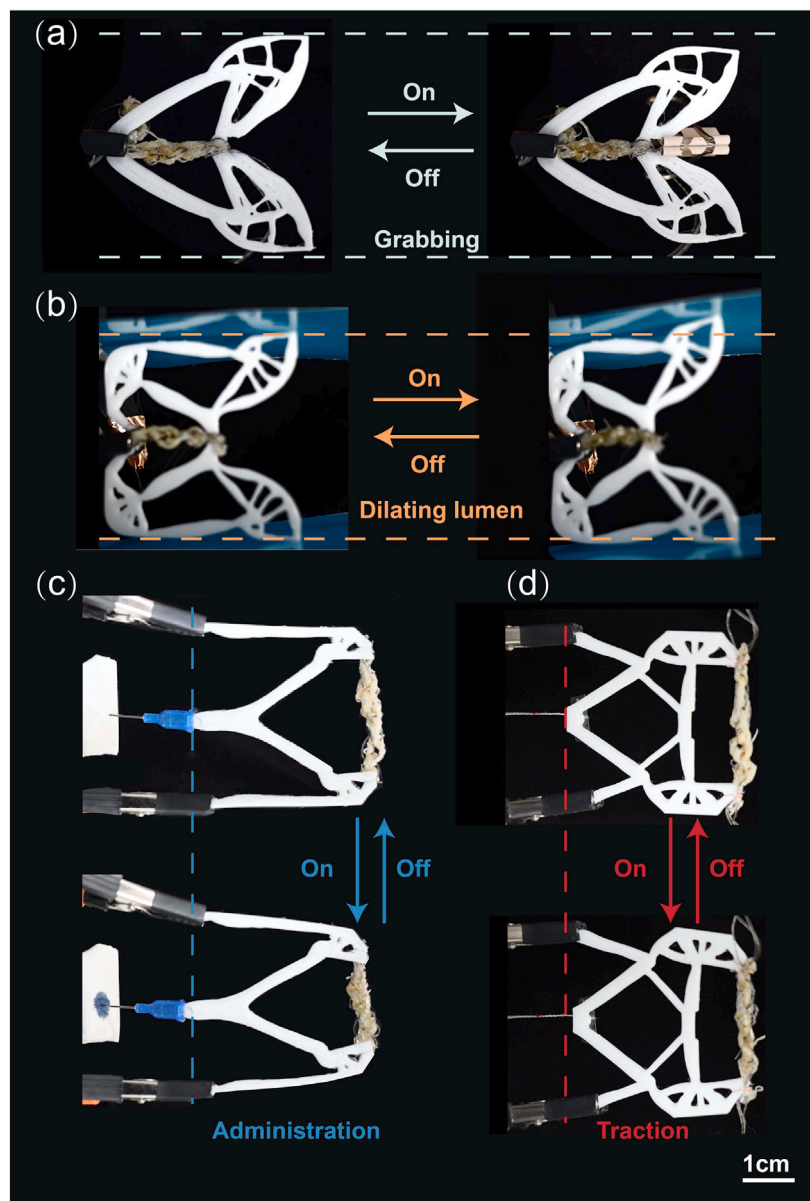


**Fig. 11. Surgical application of active compliant mechanisms with remote stimulation of current.** (a) The grabbing process of active compliant mechanism A. (b) The dilating process of active compliant mechanism B. (c) The administration process of active compliant mechanism C. (d) The traction process of active compliant mechanism D.

#### CRediT authorship contribution statement

**Wenhui Chen:** Conceptualization, Data curation, Formal analysis, Investigation, Methodology, Visualization, Writing – original draft, Writing – review & editing. **Ruicheng Wang:** Investigation, Methodology, Visualization, Writing – review & editing. **Ke Liu:** Conceptualization, Project administration, Supervision, Visualization, Writing – review & editing.

#### Declaration of competing interest

The authors declare the following financial interests/personal relationships which may be considered as potential competing interests: Ke Liu reports financial support was provided by Ministry of Industry and Information Technology of the People's Republic of China. If there are other authors, they declare that they have no known competing financial interests or personal relationships that could have appeared to influence the work reported in this paper.

#### Data availability

Data will be made available on request.

#### Acknowledgments

This research is supported by the National Key Research and Development Program of China through grant 2022YFB4701900, and the College of Engineering of Peking University.

#### Appendix A. Supplementary data

Supplementary material related to this article can be found online at <https://doi.org/10.1016/j.mechmat.2023.104879>.

#### References

- Andreassen, E., Clausen, A., Schevenels, M., Lazarov, B.S., Sigmund, O., 2011. Efficient topology optimization in MATLAB using 88 lines of code. *Struct. Multidiscipl. Optim.* 43, 1–16.

- Ansola, R., Veguería, E., Maturana, A., Canales, J., 2010. 3D compliant mechanisms synthesis by a finite element addition procedure. *Finite Elem. Anal. Des.* 46 (9), 760–769.
- Aaromni, O.A., Graule, M.A., Dorsey, K.L., Castellanos, S., Foster, J.R., Hsu, W.-H., Passy, A.E., Vlassak, J.J., Weaver, J.C., Walsh, C.J., Wood, R.J., 2020. Ultra-sensitive and resilient compliant strain gauges for soft machines. *Nature* (7833), 219–224.
- Bendsøe, M.P., Sigmund, O., 2004. Topology Optimization Theory, Methods, and Applications. Springer Nature.
- Bharti, S., Frecker, M., 2008. Compliant mechanical amplifier design using multiple optimally placed actuators. In: ASME International Mechanical Engineering Congress and Exposition. ASME, pp. 139–146.
- Bisoyi, H.K., Li, Q., 2022. Liquid crystals: Versatile self-organized smart soft materials. *Chem. Rev.* 122 (5), 4887–4926.
- Chandrasekhar, K., Bhikshma, V., Mohi, S.A., 2019. On the six node hexagon elements for continuum topology optimization of plates carrying in plane loading and shell structures carrying out of plane loading. *J. Appl. Comput. Mech.* 6, 617–639.
- Chen, Y., Li, J., Zhu, J., 2022. Topology optimization of quantum spin Hall effect-based second-order phononic topological insulator. *Mech. Syst. Signal Process.* 164, 108243.
- Chen, F., Song, Z., Chen, S., Gu, G., Zhu, X., 2023. Morphological design for pneumatic soft actuators and robots with desired deformation behavior. *IEEE Trans. Robot.* 39 (6), 4408–4428.
- Chen, W., Xia, L., Yang, J., Huang, X., 2018. Optimal microstructures of elastoplastic cellular materials under various macroscopic strains. *Mech. Mater.* 118, 120–132.
- Fowler, R., Howell, L., Magleby, S., 2011. Compliant space mechanisms: a new frontier for compliant mechanisms. *Mech. Sci.* 2, 205–215.
- Fu, L., Zhao, W., Ma, J., Yang, M., Liu, X., Zhang, L., Chen, Y., 2022. A humidity-powered soft robot with fast rolling locomotion. *Research* 2022, 2022/9832901.
- He, Q., Wang, Z., Wang, Y., Wang, Z., Li, C., Annapooranan, R., Zeng, J., Chen, R., Cai, S., 2021. Electrospun liquid crystal elastomer microfiber actuator. *Science Robotics* 6 (9), eabi9704.
- Howell, L.L., 2012. Compliant mechanisms. In: 21st Century Kinematics. Springer, pp. 189–216.
- Javadzadeh, M., del Barrio, J., Sanchez-Somolinos, C., 2023. Melt electrowriting of liquid crystal elastomer scaffolds with programmed mechanical response. *Adv. Mater.* 35, 2209244.
- Jia, Y., Lopez-Pamies, O., Zhang, X.S., 2023. Controlling the fracture response of structures via topology optimization: From delaying fracture nucleation to maximizing toughness. *J. Mech. Phys. Solids* 173, 105227.
- Karakus, R., Tanik, E., 2018. Novel compliant wiper mechanism. *Mech. Sci.* 9, 327–336.
- Ke, Y., Zhou, C., Zhou, Y., Wang, S., Chan, S.H., Long, Y., 2018. Emerging thermal-responsive materials and integrated techniques targeting the energy-efficient smart window application. *Adv. Funct. Mater.* 28 (22), 1800113.
- Kim, H., Boothby, J.M., Ramachandran, S., Lee, C.D., Ware, T.H., 2017. Tough, shape-changing materials: Crystallized liquid crystal elastomers. *Macromolecules* 50, 4267–4275.
- Kim, I.H., Choi, S., Lee, J., Jung, J., Yeo, J., Kim, J.T., Ryu, S., kyun Ahn, S., Kang, J., Poulin, P., Kim, S.O., 2022. Human-muscle-inspired single fibre actuator with reversible percolation. *Nat. Nanotechnol.* 17, 1198–1205.
- Kim, Y.-J., Matsunaga, Y.T., 2017. Thermo-responsive polymers and their application as smart biomaterials. *J. Mater. Chem. B* 5, 4307–4321.
- Kota, S., Lu, K.-J., Kreiner, Z., Trease, B., Arenas, J., Geiger, J., 2005. Design and application of compliant mechanisms for surgical tools. *J. Biomech. Eng.* 127, 981–989.
- Kotikian, A., Morales, J., Lu, A., Mueller, J., Davidso, Z., Boley, J., Lewis, J., 2021. Innervated, self-sensing liquid crystal elastomer actuators with closed loop control. *Adv. Mater.* 33, 2101814.
- Langelaar, M., 2016. Topology optimization of 3D self-supporting structures for additive manufacturing. *Addit. Manuf.* 12, 60–70.
- Li, W., Wang, F., Sigmund, O., Zhang, X.S., 2022. Digital synthesis of free-form multi-material structures for realization of arbitrary programmed mechanical responses. *Proc. Natl. Acad. Sci. USA* 119, e2120563119.
- Li, W., Zhang, X.S., 2023. Arbitrary curvature programming of thermo-active liquid crystal elastomer via topology optimization. *Comput. Methods Appl. Mech. Eng.* 417, 116393.
- Liu, C.-H., Chiu, C.-H., Hsu, M.-C., Chen, Y., Chiang, Y.-P., 2019a. Topology and size-shape optimization of an adaptive compliant gripper with high mechanical advantage for grasping irregular objects. *Robotica* 37 (8), 1383–1400.
- Liu, C.-H., Chiu, C.-H., Hsu, M.-C., Yang, C., Chiang, Y.-P., 2019b. Topology and size-shape optimization of an adaptive compliant gripper with high mechanical advantage for grasping irregular objects. *Robotica* 37, 1383–1400.
- Liu, K., Hacker, F., Daraio, C., 2021. Robotic surfaces with reversible, spatiotemporal control for shape morphing and object manipulation. *Science Robotics* 6 (53), eaef5116.
- Liu, K., Paulino, G.H., 2019. Tensegrity topology optimization by force maximization on arbitrary ground structures. *Struct. Multidiscip. Optim.* 59 (6), 2041–2062.
- Liu, K., Tovar, A., 2014. An efficient 3D topology optimization code written in Matlab. *Finite Elem. Anal. Des.* 50 (6), 1175–1196.
- Lu, Y., Aimetti, A.A., Langer, R., Gu, Z., 2016. Bioresponsive materials. *Nat. Rev. Mater.* 2 (1), 16075.
- Mackertich-Sengerdy, G., Campbell, S.D., Werner, D.H., 2023. Tailored compliant mechanisms for reconfigurable electromagnetic devices. *Nature Commun.* 14, 683.
- Madden, J., Vandesteeg, N., Anquetil, P., Madden, P., Takshi, A., Pytel, R., Lafontaine, S., Wieringa, P., Wieringa, P., 2004. Artificial muscle technology: physical principles and naval prospects. *IEEE J. Ocean. Eng.* 29 (3), 706–728.
- Odhner, L.U., Jentoft, L.P., Claffee, M.R., Corson, N., Tenzer, Y., Ma, R.R., Buehler, M., Kohout, R., Howe, R.D., Dollar, A.M., 2014. A compliant, underactuated hand for robust manipulation. *Int. J. Robot. Res.* 33 (5), 736–752.
- Pereira, A., Menezes, I., Talischi, C., Paulino, G., 2011. An efficient and compact MATLAB implementation of topology optimization: Application to compliant mechanisms.
- Roach, D.J., Yuan, C., Kuang, X., Li, V.C.-F., Blake, P., Romero, M.L., Hammel, I., Yu, K., Qi, H.J., 2019. Long liquid crystal elastomer fibers with large reversible actuation strains for smart textiles and artificial muscles. *ACS Appl. Mater. Inter.* 11, 19514–19521.
- Sigmund, O., 2001. A 99 line topology optimization code written in matlab. *Struct. Multidiscipl. Optim.* 21, 120–127.
- Soto, F., Karshalev, E., Zhang, F., Esteban Fernandez De Avila, B., Nourhani, A., Wang, J., 2022. Smart materials for microrobots. *Chem. Rev.* 122 (5), 5365–5403.
- Talischi, C., Paulino, G.H., Pereira, A., Menezes, I.F.M., 2012a. PolyTop: a matlab implementation of a general topology optimization framework using unstructured polygonal finite element meshes. *Struct. Multidiscipl. Optim.* 45, 329–357.
- Talischi, C., Paulino, G.H., Pereira, A., Menezes, I.F.M., 2012b. PolyMesher: a general-purpose mesh generator for polygonal elements written in matlab. *Struct. Multidiscipl. Optim.* 45, 309–328.
- Tang, L., Wang, L., Yang, X., Feng, Y., Li, Y., Feng, W., 2021. Poly(N-isopropylacrylamide)-based smart hydrogels: Design, properties and applications. *Prog. Mater. Sci.* 115, 100702.
- Thomas, T.L., Kalpathy Venkiteswaran, V., Ananthasuresh, G.K., Misra, S., 2021. Surgical applications of compliant mechanisms: A review. *J. Mech. Robot.* 13, 020801.
- Wallin, M., Tortorelli, D.A., 2020. Nonlinear homogenization for topology optimization. *Mech. Mater.* 145, 10324.
- Wang, Y., He, Q., Wang, Z., Zhang, S., Li, C., Wang, Z., Park, Y.-L., Cai, S., 2023. Liquid crystal elastomer based dexterous artificial motor unit. *Adv. Mater.* 202211283.
- Wang, Q., Yu, L., Yu, M., Zhao, D., Song, P., Chi, H., Guo, L., Yang, H., 2017. Liquid crystal elastomer actuators from anisotropic porous polymer template. *Macromol. Rapid Commun.* 38, 1600699.
- Weng, W., Chen, P., He, S., Sun, X., Peng, H., 2016. Smart electronic textiles. *Angew. Chem. Int. Edn* 55 (21), 6140–6169.
- Wu, S., Hong, Y., Zhao, Y., Yin, J., Zhu, Y., 2023. Caterpillar-inspired soft crawling robot with distributed programmable thermal actuation. *Sci. Adv.* 9.
- Wu, J., Yao, S., Zhang, H., Man, W., Bai, Z., Zhang, F., Wang, X., Fang, D., Zhang, Y., 2021. Liquid crystal elastomer metamaterials with giant biaxial thermal shrinkage for enhancing skin regeneration. *Adv. Mater.* 33, 2106175.
- Ying, B., Chen, R.Z., Zuo, R., Li, J., Liu, X., 2021. An anti-freezing, ambient-stable and highly stretchable ionic skin with strong surface adhesion for wearable sensing and soft robotics. *Adv. Funct. Mater.* 31 (42), 2104665.
- Yu, X., Cheng, H., Zhang, M., Zhao, Y., Qu, L., Shi, G., 2017. Graphene-based smart materials. *Nat. Rev. Mater.* 2 (9), 17046.
- Yu, H., Guo, Y., Yao, C., Perepichka, D.F., Meng, H., 2016. A smart polymer with a high sensitivity to temperature and humidity based on polyacrylamide hydrogel doped with polyiodide. *J. Mater. Chem. C* 4 (47), 11055–11058.
- Zhang, X.S., Paulino, G.H., Ramos, A.S., 2018. Multi-material topology optimization with multiple volume constraints: a general approach applied to ground structures with material nonlinearity. *Struct. Multidiscipl. Optim.* 57 (1), 161–182.
- Zhang, W., Zhou, L., 2018. Topology optimization of self-supporting structures with polygon features for additive manufacturing. *Comput. Methods Appl. Mech. Engrg.* 334, 56–78.
- Zhang, X., Zhu, B., 2018. Topology Optimization of Compliant Mechanisms. Springer.
- Zhu, B., Zhang, X., Wang, N., 2018. Topology optimization of hinge-free compliant mechanisms with multiple outputs using level set method. *Struct. Multidiscipl. Optim.* 47, 659–672.
- Zhu, B., Zhang, X., Zhang, H., Liang, J., Zang, H., Li, H., Wang, R., 2020. Design of compliant mechanisms using continuum topology optimization: A review. *Mech. Mach. Theory* 143, 103622.
- Zirbel, S.A., Tolman, K.A., Trease, B.P., Howell, L.L., 2017. Bistable mechanisms for space applications. *PLoS One* 11, e0168218.